THERMAL FIELD AND RESIDUAL STRESSES DURING THE RESISTANCE SPOT WELDING PROCESS

Dan Birsan[1]

[1] *"Dunarea de Jos" University of Galati, dbirsan@ugal.ro.*

Abstract: *The main reason why the resistance spot welding process is mainly used in the automotive and supplier industries is its wide range of applications. The resistance welding process greatly affects the localization of the material, so its monitoring is very important. Process monitoring and quality assurance can be easily completed during the welding process. Resistance spot welding is based on the generation of Joule heat. The 3D FEM model, two plates (80x25x1mm) and two weld guns (copper electrodes, B0-13-18-30-5-31, according to ISO 5821), has been modeled in order to simulate the resistance spot welding process. The material used for plates is 316LNSPH, an austenitic stainless steel.*

Keywords: *resistance spot weld, finite element, stress*

1. Introduction

Many papers have been written on various aspects of simulation, modelling and process optimization in the resistance spot welding process of steel. In these works, detailed analysis established relationship welding parameters, welding strength, welding quality and select the productivity of welding parameters for an optimal process. This process involves strong interactions between electrical, thermal, metallurgical and mechanical the areas summarized in Figure 1. In terms of simulation, solving each time steps are obtained based on mechanical analysis Followed by electro thermal metallurgy analyze. In this article, the discussion will focus on electro thermal coupling modeling. More information about mechanical coupling can be found in Refs. [1,2,3]. A lot of work has been done to simulate heat contact by finite element method. Most methods consider thin layers of elements model the contact properties Ref. [4]. For others method, the electric contact condition is by connecting the elements facing the two nodes Refs. [1,5]. In this case, the relative displacement due to the mechanical analysis in the welding process cannot be explained easily and restrictions due to this geometrical assumption involve large difficulties for meshing electrodes and sheets.

The first part of the article will detail the general formulation of electro thermal contact conditions between the electrode and the sheet. The second part of this article will discuss simulation welding of two steel plates.

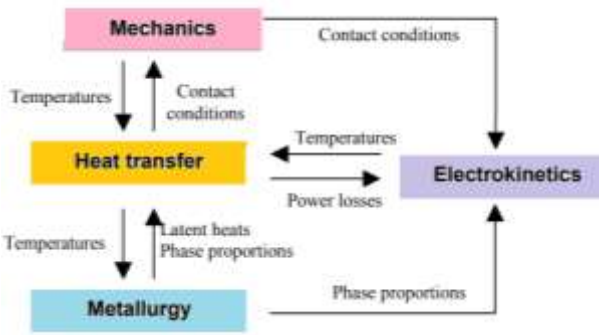

Figure 1: *Couplings between metallurgy, mechanics electro kinetics and heat transfer*

The joule heating effect converts the electrical energy into heat energy and for an electrical current the heat flux is calculated as shown below:

$$\boldsymbol{Q = R \cdot I^2} \qquad (1)$$

In simulation of the welding process the electrical contact conductivity has been calculated automatically with the following formula, according to Bay and Wanheim:

$$\boldsymbol{q = 3 \cdot \left(\frac{\sigma_{soft}}{\sigma_n}\right) \cdot \left(\frac{\rho_1+\rho_2}{2}\right) + \rho_c} \qquad (2)$$

where:

- σ_{soft} - flow stress of the softer material (temperature dependent);
- σ_n - contact normal stress;
- ρ_1, ρ_2 - resistivity of the contact partners (temperature and phase dependent);
- ρ_c - resistivity of coatings (optional).

In most cases, the contact resistance is 30 times greater than the material resistance. Electrical appliances material resistance and electrical contact resistance strongly depend on temperature. Electrical contacts resistance is also related to contact pressure. During the welding process, the contact resistance decreases rapidly due to the compression of the sheet and the material resistance increases due to the increase temperature. After welding, the resistance of the material decreases during the cooling process. The Fig. 2 shows the electricity contact resistance, material resistance and the complete resistance of the system during welding including subsequent cooling.

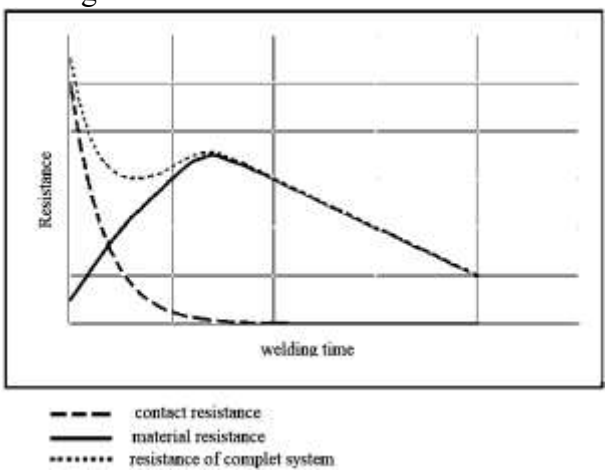

Figure 2: *Electrical resistances during a resistance welding process (welding and cooling)*

2. Numerical Model Development

In the case of welding by resistance spot, temperature field profile depends on primary welding parameters - voltage, amperage, welding speed - thermo-physical properties of the base material - specific heat, thermal conductibility, thermal diffusivity, mass density and heat loss by convection and radiation.

For a complete definition of a resistance welding process a closed electrical circuit has been constructed. The electrical circuit has been closed with a rigid body with a defined electrical current and a rigid body as a defined electrical potentials of 0V have electrical contact to the remaining electrical circuit. The rigid body with the electrical potential of 0 V acts like ground and the other rigid body acts like an electrode.

The 3D finite elements model consists by two plates (80x25x1mm) and two weld guns (copper electrodes, B0-13-18-30-5-31, according to ISO 5821), as shown Fig. 3. The mesh is fine around these weld lines, and coarse in the far field.

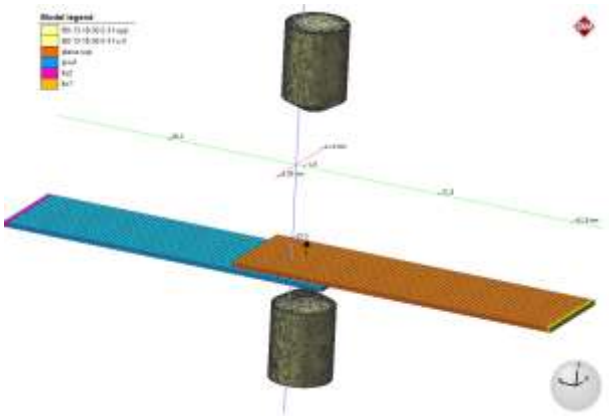

Figure 3: *3D finite elements model*

The plates have been constrained with bearing and clamping in order to simulate the real physic process.

In this model, the electrical material resistance has been entered depending on temperature and material phase.

Due to the fact that the electrical resistivity is the reciprocal of the electrical conductivity an automatic conversion from one to the other is done. The electrical material parameters have been provided for all materials of the material library.

The Fig. 4 shows the electrical material resistivity of S235 steel.

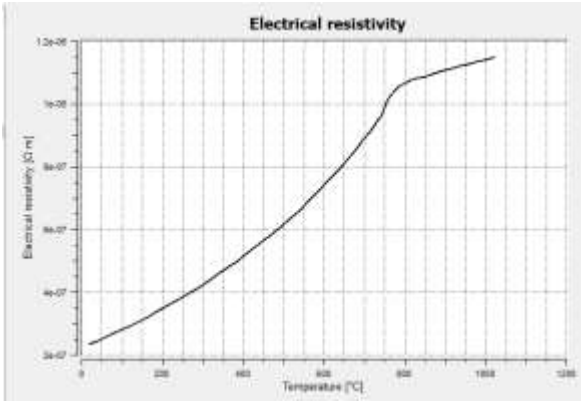

Figure 4: *Definition of the electrical material resistivity*

Values of temperatures and of the flux gradients are predicted in the entire welded joint but still, they are particularly pursued in and around the fusion zone (FZ) and heat affected zone (HAZ), where metallurgical and mechanical properties have been seriously modified. The heat transfer in the structure was modelled as 3D heat transfer problem using the Simufact Welding software. S235-JMP-MPM low carbon steel has been used in this simulation. Table 1 show the S235 chemical composition.

Table 1: *S235 chemical composition (%)*

C	Cu	Fe	Mn	N	P	S
0.15	0.4	98.293	1.1	0.01	0.02	0.027

The Clamp force table (Fig. 5) and the Electrical current table (Fig. 6) have been entered in model. Both tables are time dependent. The welding time in this simulation is 1.0s. In this time the clamp force should stay constant at 1700N.

The maximum electrical current is 4000A and should be activated shortly after the clamp force is active.

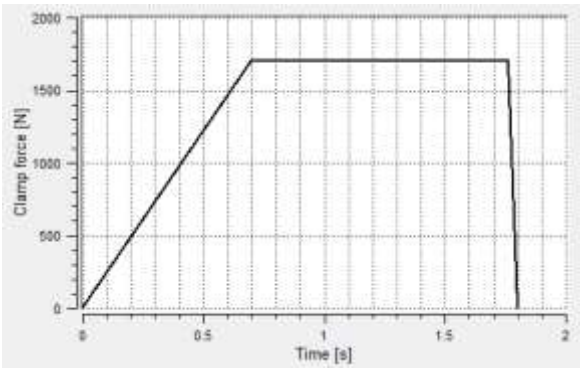

Figure 5: *Clamp force during the resistance welding process*

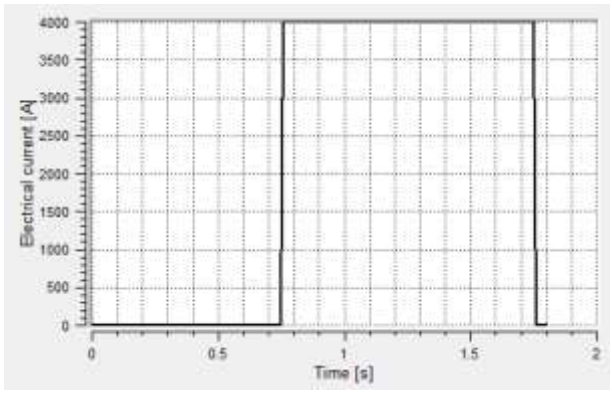

Figure 6: *Electrical current during the resistance welding process*

The numerical model has been made, taking into consideration the following assumptions:

- isotropy of the base metal;
- thermo-physical properties dependent on temperature;
- convection and radiation losses;
- latent heat;
- phase transformation.

3. Results and Discussions

3.1. Temperature field distribution

Modeling, simulation and analysis of thermal fields were performed taking into account all the assumptions and conditions specified in chapter 2.

In Figs. 7,8,9 there are presented the distributions of the thermal fields, generated by the welding source at 0.864 and 0.936 seconds from the beginning of the welding process.

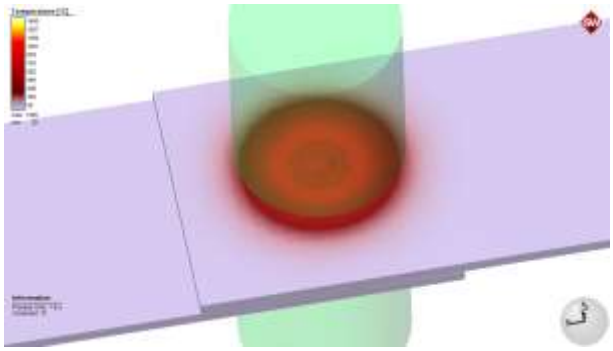

Figure 7: *Thermal field at 0.864s*

For the case of heat sources, the simulation of heat transfer in welded joints requires a fine mesh of a sufficiently wide area to include

thermal effects, around the hot spot of the two parts to be welded. For austenitic steel have been analyzed the isotherms of AC1 and AC3 temperature and the phase fraction of ferrite, pearlite, austenite, bainite and martensite at a certain point in the welding process.

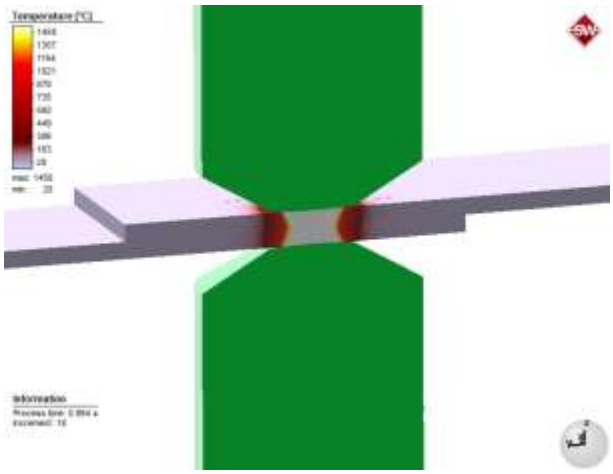

Figure 8: *Cross section through the molten metal pool at 0.864s*

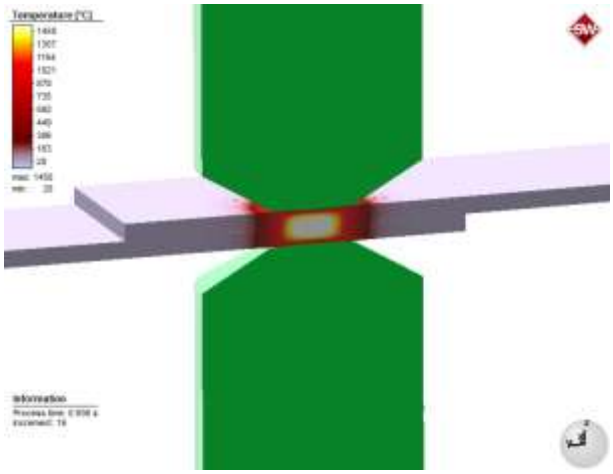

Figure 9: *Cross section through the molten metal pool at 0.936s*

The temperature variations over time of the selected nodes (see Fig. 10) from the top plate and bottom plates are shown in Figs. 11,12. Can be observed the maximum temperature reached during the welding process for both locations. The distance between two nodes is 1 mm.

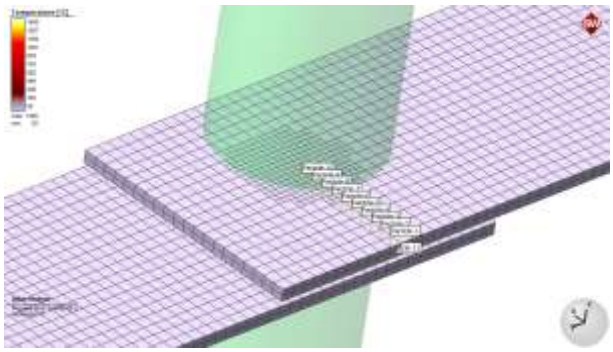

Figure 10: *Selected nodes on plates for monitoring the temperature and stresses*

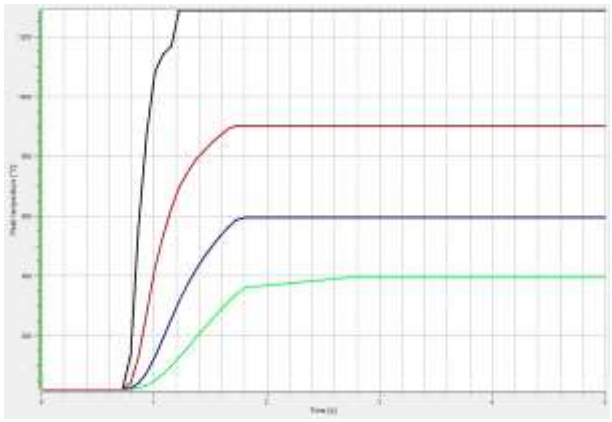

Figure 11: *Thermal cycle in nodes of top plate*

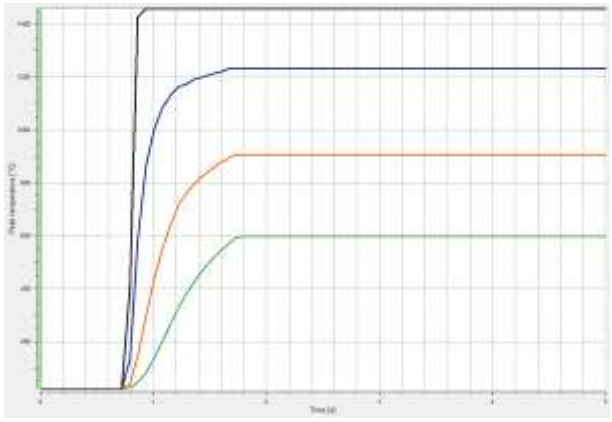

Figure 12: *Thermal cycle in nodes located at the interface between plates*

3.2. Von Mises Stresses Distribution

Welding stress modeling includes all deformations that can be predicted by thermal stress analysis. Most thermal stress analysis uses a thermo-elasto-plastic constitutive model with rate-independent plasticity. In Figs. 13,14 it can be observed the effective stresses in the welded joint for two moments of time, during and after welding process. The effective stress of a welded joint depends on its temperature. It

can be noticed that the maximum stress occurs in the heat affected zone (HAZ), the red area in Figs. 13,14,15,16 the maximum equivalent stress being about 270MPa during welding process. The residual stresses in plates are 360MPa.

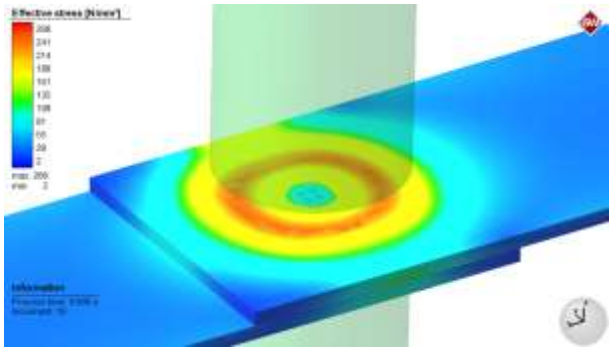

Figure 13: *Effective stresses distribution in plates at 0.936s*

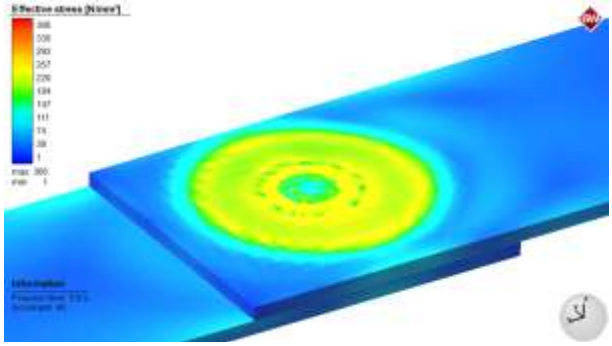

Figure 14: *Residual stresses distribution in plates*

In Figs. 15,16 it can be observed the effective stresses in the welded joint – cross section for two moments of time, during and after welding process.

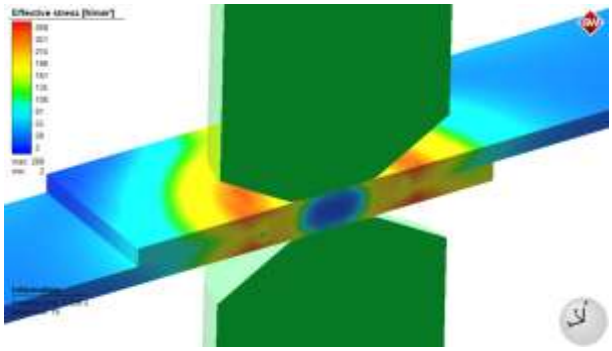

Figure 15: *Effective stresses distribution at 0.936s - Cross section*

The effective stresses in nodes of top plate and at the interface between plates are shown in the graphs in Figs. 17 and 18.

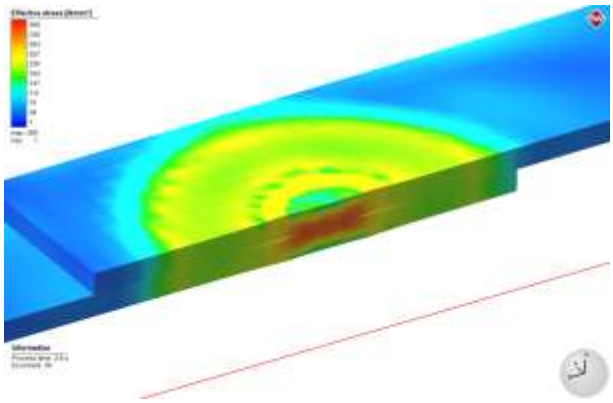

Figure 16: *Residual stresses - Cross section*

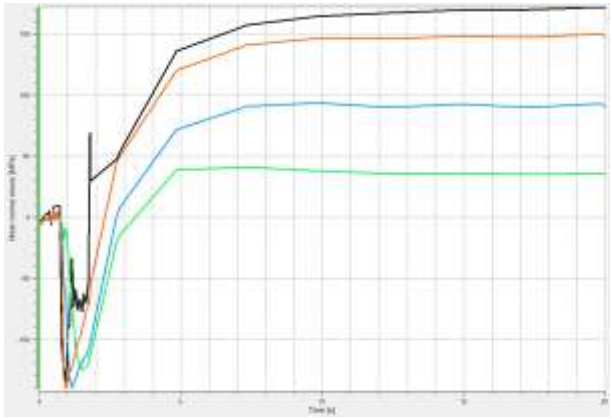

Figure 17: *Effective stress in nodes of top plate*

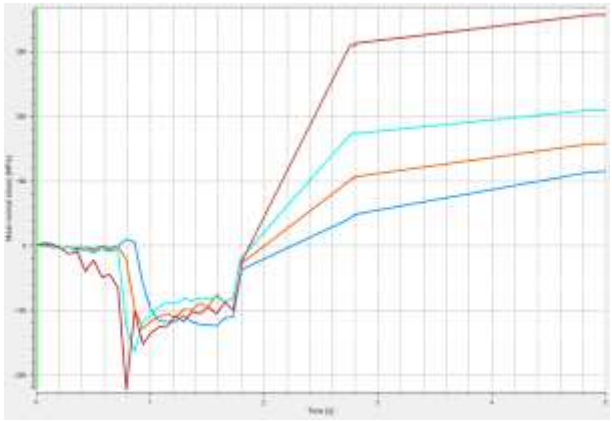

Figure 18: *Effective stress in nodes located at the interface between plates*

4. Conclusions

The welding simulation takes into account the changes in the thermo-physical and mechanical properties of S235 steel with temperature, which leads to a very accurate solution regarding the distribution and value of the thermal field and residual stress. In this welding simulation, the phase change of the material under consideration is very important.

Three-dimensional analysis provides us with important data about the shape of the molten pool and the isotherms of the thermal field. The maximum value of the equivalent stress corresponds to the heat-affected zone. The increase in residual stress only occurs after the structural transformation is completed.

References

1. [Deng, 2020], Deng L., Li Y. B., Cai W., Haselhuhn A. and Carlson B., *Simulating Thermoelectric Effect and Its Impact on Asymmetric Weld Nugget Growth in Aluminum Resistance Spot Welding*, Journal of Manufacturing Science and Engineering, Volume 142, Issue 9, 2020.
2. [Cai, 2019], Cai W., Daehn G., Vivek, A., Li J., Khan H., Mishra R. S., and Komarasamy M., *A State-of-the-Art Review on Solid-State Metal Joining*, ASME J. Manuf. Sci. Eng., 141(3).
3. [Gould, 2014], Gould J., *Challenges and Advances in Resistance Spot Welding Aluminum Sheet*, EWI Report, April 28, 2014.
4. [Zhao 2020],Zhao D., Ivanov M., Wang Y., Liang D. and Du W., *Multi-objective optimization of the resistance spot welding process using a hybrid approach*, Journal of Intelligent Manufacturing, 2020.
5. [Amaral 2018], Amaral F. F., Almeida F. A. D., Costa S. C., Leme R. C. and Paiva, A. P. D., *Application of the response surface methodology for optimization of the resistance spot welding process in AISI 1006 galvanized steel*, Soldagem & Inspeção,23, 129–142.
6. [Chen 2017], Chen F., Tong G. Q., Yue X., Ma X., and Gao, X., *Multi-performance optimization of small-scale resistance spot welding process parameters for joining of Ti–1Al–1Mn thin foils using hybrid approach*, The International Journal of Advanced Manufacturing Technology,89, 3641–3650, 2017.
7. [Dhawale 2019], Dhawale P. A., and Ronge B. P., *Parametric optimization of resistance spot welding for multi spot welded lap shear specimen to predict weld strength*, Materials Today: Proceedings,19, 700–707, 2019.
8. [Ghazali 2015], Ghazali, F. A., Berhan, M. N., Manurung, Y. H., Salleh, Z., and Abdullah S., *Tri-objective optimization of carbon steel spot-welded joints*, Jurnal Teknologi,76, 69–73, 2015.
9. [Khuenkaew 2019], Khuenkaew T., and Kanlayasiri K., *Resistance spot welding of SUS316L austenitic/SUS425 ferritic stainless steels: weldment characteristics, mechanical properties, phase transformation and solidification*. Metals, 9, 710, 2019.
10. [Kınagu 2018], Kınagu H. M., Gökçedağlıoğlu M., Ateş F., Küçükelyas B., Mutlu M., Erhuy C. G., et al., *Suggestion of an indicator to evaluate material deposition in resistance spot welding: weld-surface interaction index*, Journal of Materials Engineering and Performance, 27, 5086–5094, 2018.